photonics

MDPI

Article

Simultaneous Ce Ion Doping in Core and Cladding to Enhance the Radiation Resistance of Erbium-Doped Fibers

Yangjian Xu [1,2,3], Ziyang Xiao [2], Wenju Feng [1,2,3], Ruixiang Fan [2], Tao Yang [2] and Wei Chen [1,2,3,*]

[1] Key Laboratory of Specialty Fiber Optics and Optical Access Networks, Shanghai University, Shanghai 200444, China
[2] State Grid Jiangxi Electric Power Co., Ltd., Nanchang 330077, China
[3] Institute of Fiber Optics, Shanghai University, Shanghai 200444, China
* Correspondence: chenweisd@shu.edu.cn

Abstract

Erbium-doped fibers (EDFs) suffer from radiation-induced absorption (RIA) and radiation-induced gain variation (RIGV) under ionizing radiation, which limit their applications in space optical communication systems. To address this issue, a novel core–cladding Ce co-doped fiber is proposed, in which core Ce suppresses radiation-induced defect formation while cladding Ce reduces localized energy deposition in the fiber core. GEANT4 Monte Carlo simulations were performed to optimize the Ce-doping configuration, and three kinds of fiber samples, namely conventional erbium-doped fiber (EDF), core Ce co-doped EDF (CEDF1), and core–cladding Ce co-doped EDF (CEDF2), were fabricated for experimental validation. At a total dose of 1200 Gy, CEDF2 exhibits a 40.5% reduction in RIA and a 58.1% reduction in RIGV compared with the conventional EDF. The experimental results demonstrate that the proposed core–cladding Ce co-doped structure effectively enhances the radiation resistance of erbium-doped fibers and provides a practical design strategy for radiation-hardened active optical fibers.

Keywords: erbium-doped fiber; radiation resistance; Ce co-doping; radiation-induced absorption

1. Introduction

Erbium-doped fibers (EDFs) have become key active optical components owing to their excellent amplification performance in the 1550 nm communication window. Their importance has further increased with the rapid development of space optical communication systems, where they serve as the gain medium in fiber amplifiers and other active photonic devices [1–5]. However, the space environment presents unique challenges for the long-term reliability of these technologies. For instance, the Earth is surrounded by the Van Allen radiation belts, where spacecraft are exposed to various types of harsh radiation [6]. The energetic particles trapped in the radiation belts can cause severe radiation damage to optical fiber devices, leading to radiation-induced absorption (RIA) and radiation-induced gain variation (RIGV), thereby degrading the performance and long-term reliability of fiber-optic communication systems [7–9].

To improve the radiation resistance of optical fibers, researchers have proposed various methods, including gas loading, photobleaching, and optimization of fiber composition and dopant distribution [10–12]. Although these approaches have demonstrated effectiveness in mitigating radiation-induced degradation, each has inherent limitations. Gas loading

Check for updates

Received: 27 June 2026
Revised: 19 July 2026
Accepted: 29 July 2026
Published: 31 July 2026

Copyright: © 2026 by the authors. Licensee MDPI, Basel, Switzerland. This article is an open access article distributed under the terms and conditions of the Creative Commons Attribution (CC BY) license.

generally requires additional processing and may suffer from gas diffusion and long-term stability issues. Photobleaching relies on external optical excitation and is therefore difficult to maintain during continuous operation. Material modification through rare-earth co-doping offers a more permanent solution, but most existing studies have primarily focused on suppressing radiation-induced defect formation within the fiber core rather than regulating the spatial distribution of radiation energy deposition. Cerium (Ce) co-doping has attracted broad attention due to reversible valence state conversion between Ce^{3+} and Ce^{4+} [13,14]. Jiao et al. [15] found that Ce^{3+} ions can neutralize radiation-induced holes to form Ce^{4+}-related centers, thereby preventing the formation of aluminum oxygen hole centers (Al-OHCs). Ce^{4+} ions capture radiation-induced free electrons and are converted back to Ce^{3+}, inhibiting the formation of Si-E′ and Al-E′ defect centers and consequently suppressing the growth of RIA. Girard et al. [16] further demonstrated that Ce co-doping significantly improved the radiation resistance of erbium-doped fibers and fiber amplifiers. However, previous studies have mainly focused on Ce incorporation within the fiber core [17,18], while the effects of Er/Ce co-doping concentration and cladding Ce design on particle transport and energy deposition have not been systematically investigated. Therefore, engineering the spatial distribution of Ce in both the core and cladding provides a potential strategy for further improving the radiation resistance of erbium-doped fibers.

At present, the radiation resistance of optical fibers is mainly evaluated through γ-ray irradiation experiments. The optimization of radiation-resistant fiber structures and compositions primarily relies on experimental observations and performance characterization. In recent years, Monte Carlo simulation has become an effective tool for analyzing radiation–matter interactions and guiding the design of radiation-resistant optical fibers. GEANT4, a Monte Carlo simulation toolkit developed by the European Organization for Nuclear Research (CERN), has been widely utilized to simulate particle transport and energy deposition processes in radiation-related studies [19]. Unlike experimental irradiation tests, Monte Carlo simulations can directly reveal particle transport and spatial energy-deposition processes that are difficult to measure experimentally. Accordingly, GEANT4 provides an effective tool for investigating how different Ce-doping configurations influence radiation energy deposition and for guiding the optimization of radiation-resistant fiber structures. In this work, GEANT4 was employed to establish γ-ray irradiation models of conventional EDF, core Ce co-doped EDF (CEDF1), and core–cladding Ce co-doped EDF (CEDF2) to investigate the influence of different Ce-doping configurations on the radiation resistance of erbium-doped fibers. A series of simulations was performed to evaluate the effects of Er/Ce concentration ratio, cladding Ce concentration, and cladding thickness on energy deposition behavior. EDF, CEDF1, and CEDF2 were fabricated using the modified chemical vapor deposition (MCVD) process combined with solution doping. The fabricated fibers were subsequently exposed to ^{60}Co γ-ray irradiation. Their radiation resistance was evaluated by measuring the absorption spectra, gain spectra, RIA, and RIGV. By combining GEANT4 simulations with experimental validation, this work aims to establish a structure-guided strategy for developing radiation-hardened erbium-doped fibers for future space optical communication systems.

2. Materials and Methods

2.1. Radiation Damage Mechanisms

The interaction of γ-rays with optical fiber materials mainly involves three processes: the photoelectric effect, the Compton effect, and electron–positron pair production [7]. The probability of each process depends on its corresponding interaction cross-section. In general, elements with higher atomic numbers exhibit larger interaction cross-sections and are therefore more likely to interact with incident γ-rays. Their energy is first transferred to

secondary electrons through these interaction processes. The generated secondary electrons subsequently induce ionization and defect formation within the material. These defects are responsible for radiation-induced degradation in optical fibers [20].

The growth of RIA is primarily related to the irradiation dose rate and the accumulated total dose. RIA mainly originates from defect centers associated with co-dopants in the fiber core rather than from the rare-earth ions themselves. Co-dopants are introduced to enhance the solubility of Er ions and suppress ion clustering. However, these dopants are susceptible to color-center formation after irradiation. For example, aluminum, one of the most widely used co-dopants in erbium-doped fibers, exists in the silica network mainly as $\{AlO_{4/2}\}^-$ and $\{AlO_{3/2}\}^0$ structural units [21]. Under irradiation, these precursor centers can capture radiation-induced holes and electrons, the former converts to an Al-OHC color center by capturing holes, while the latter converts to an Al-E′ color center by capturing electrons; their formation processes are shown in Equations (1) and (2) [22,23]:

$$\{AlO_{4/2}\}^- + h^+ \rightarrow \{AlO_{4/2} + h^+\}^0 (\equiv Al - O^\circ) \quad (1)$$

$$\{AlO_{3/2}\}^0 + e^- \rightarrow \{AlO_{3/2} + e^-\}^- (\equiv Al^\cdot) \quad (2)$$

These two types of defects are the primary damage mechanisms leading to the performance degradation of erbium-doped optical fibers in space irradiation environments. Since the formation of radiation-induced defect centers is driven by irradiation-generated charge carriers, reducing energy deposition within the fiber core can effectively suppress defect formation and thereby mitigate the growth of RIA.

2.2. Design of the Core–Cladding Ce Co-Doped EDF

Cerium (Ce) exhibits a multivalent characteristic and can readily undergo reversible valence transitions between Ce^{3+} and Ce^{4+} states. When the fiber core is doped with Ce, Ce^{3+}/Ce^{4+} pairs continuously trap irradiation-generated holes and electrons to hinder defect nucleation (Figure 1a). Meanwhile, the Ce-doped cladding modifies the transport behavior of radiation-induced secondary electrons and redistributes the deposited energy within the fiber structure, thereby reducing the energy deposited in the fiber core, rather than directly intercepting individual secondary electrons (Figure 1b). Therefore, Ce doping can enhance the radiation resistance of optical fibers through two complementary mechanisms: defect-center suppression via charge-carrier trapping and energy-deposition reduction through secondary-electron attenuation.

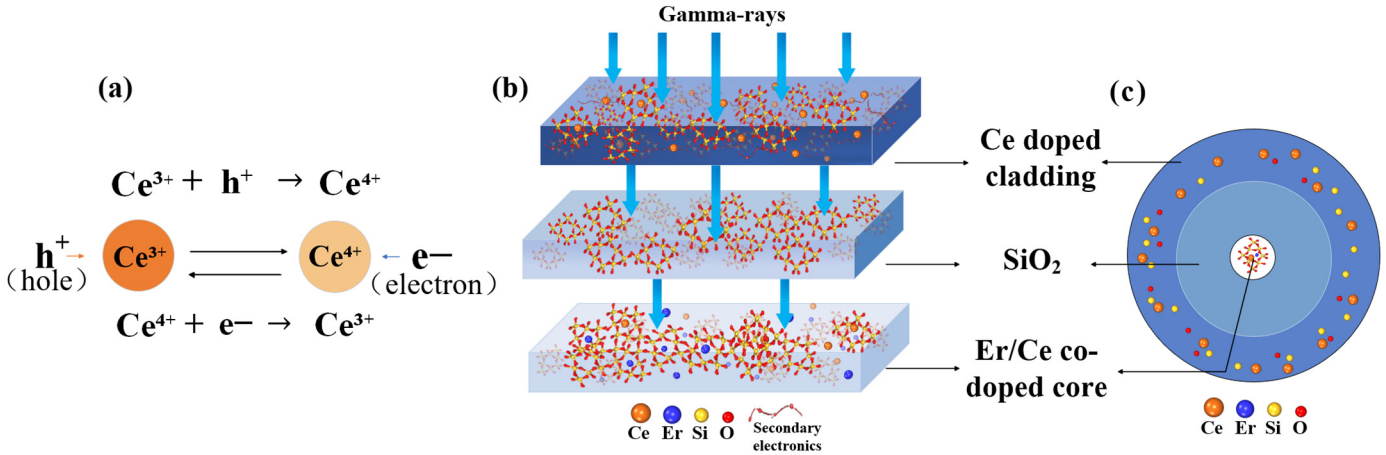


Figure 1. Schematic illustration of the proposed core–cladding Ce co-doped erbium-doped fiber and its radiation-resistance mechanisms: (**a**) reversible Ce^{3+}/Ce^{4+} valence transitions for radiation-induced

electron and hole trapping; (**b**) reduction in energy deposition in the fiber core through attenuation of secondary electrons by the Ce-doped cladding; (**c**) cross-sectional structure of the proposed core-cladding Ce co-doped fiber. The blue arrows indicate the direction of electron/hole migration and secondary-electron transport.

Based on these considerations, a novel fiber structure featuring Ce co-doping in both the fiber core and the outer cladding was designed in this work, as illustrated in Figure 1b. By combining the advantages of Ce-induced defect suppression in the core region and energy-deposition mitigation in the cladding, the proposed structure is expected to provide enhanced radiation resistance compared with conventional EDFs and core-only Ce co-doped fibers.

2.3. GEANT4 Simulation Model

Two groups of GEANT4 (Version 11.0, CERN, Geneva, Switzerland) simulation models were established to evaluate the influence of different Ce-doping configurations on the radiation resistance of erbium-doped fibers. In all simulations, a monoenergetic γ-ray source with an energy of 1.5 MeV was employed. The γ-rays were normally incident on the fiber cross section. The core and cladding radius were fixed at 4.3 μm and 62.5 μm, respectively. The concentrations of Si, O, Ge, Al, and P were kept constant in all models. A total of 1×10^6 primary photons were simulated for each condition. The electromagnetic interactions considered included the photoelectric effect, Compton scattering, and pair production. Dopants were assumed to be uniformly distributed within the corresponding regions. The total energy deposited in the fiber core and the local energy deposition around Er ions were recorded as the main scoring quantities. The main simulation conditions and model parameters are summarized in Table 1.

Table 1. Main GEANT4 simulation parameters.

Parameter	Value/Description
Radiation source	Monoenergetic γ-rays
Photon energy	1.5 MeV
Number of particles	1×10^6 photons per simulation condition
Incident direction	Normal to fiber cross section
Fiber geometry	Core radius = 4.3 μm; cladding radius = 62.5 μm
Physics processes	Photoelectric effect, Compton scattering, and pair production
Dopant distribution	Uniform distribution
Scoring quantity	Energy deposition in core & around Er ions

The simulation models were divided into two groups according to the Ce-doping configuration, as summarized in Table 2.

Table 2. GEANT4 simulation groups and doping configurations.

Fiber Group	Core Er (wt%)	Core Ce (wt%)	Cladding Ce (wt%)	Thickness of Ce Cladding (μm)
Group 1	0~1.0	0~0.5	0	0
Group 2	0.6	0.3	0~2.0	0~20

The first group of models was designed to examine the effect of Er and Ce concentrations in the fiber core on local energy deposition behavior. The Er concentration was varied from 0 to 1.0 wt% with a step size of 0.2 wt%, and the Ce concentration ranged from 0 to

0.5 wt% with a step size of 0.1 wt%. By analyzing the energy deposition in the vicinity of Er ions, the Er/Ce concentration ratio relationship between Er and Ce ions was evaluated, and the optimal core composition for radiation resistance was determined.

The second group evaluated the effect of the Ce-doped outer cladding on energy deposition using the optimized core composition identified in the first group. In this group, the core composition was fixed at 0.6 wt% Er and 0.3 wt% Ce. The Ce concentration in the outer cladding was varied from 0 to 2.0 wt% with a step size of 0.5 wt%, and the cladding thickness ranged from 0 to 20 μm with a step size of 5 μm. The second group quantified the combined effects of cladding Ce concentration and thickness on energy deposition, enabling optimization of the proposed core–cladding Ce co-doped fiber.

2.4. Simulation Results and Discussion

Figure 2 presents two-dimensional heat maps of energy deposition in the fiber core under different Er and Ce concentrations, where the color scale changes from blue to red, indicating increasing energy deposition. Figure 2a shows the total energy deposition in the fiber core for the first group of models. The total core energy deposition generally rises with increasing Er or Ce concentration. For example, when the Er concentration is fixed at 0 wt%, the total core energy deposition increases from 10.00 MeV to 13.72 MeV as the Ce concentration increases from 0 to 0.5 wt%. Similarly, when the Ce concentration is fixed at 0 wt%, the total core energy deposition increases from 10.00 MeV to 11.25 MeV as the Er concentration increases from 0 to 1.0 wt%. These results indicate that the probability of γ-ray interactions with the fiber material increases as the Er or Ce concentration increases, leading to greater energy deposition in the core and the effect of Ce concentration on energy deposition is more pronounced than that of Er concentration.

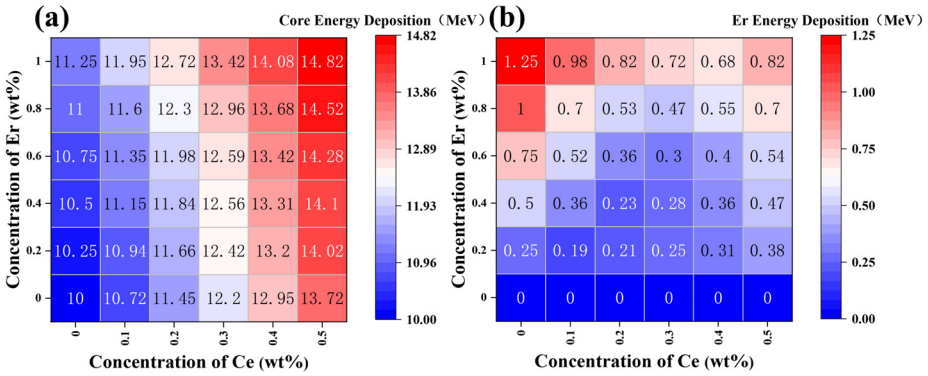


Figure 2. Two-dimensional heat maps of energy deposition under different Er and Ce concentrations: (**a**) total energy deposition in the fiber core; (**b**) Er-related energy deposition obtained by differential analysis.

However, total core energy deposition alone cannot characterize the local energy deposition around Er ions. Instead, radiation-induced gain degradation is primarily governed by the energy deposited in the vicinity of Er ions [16]. Er-related energy deposition was extracted using a differential analysis. For each Ce concentration, the energy deposition obtained with an Er concentration of 0 wt% was subtracted from the corresponding values at higher Er concentrations. The extracted Er-related energy deposition is presented in Figure 2b.

In Figure 2b, the case with a Ce concentration of 0 wt% represents the conventional EDF without Ce co-doping and serves as the reference. Compared with the Ce-free fiber, the introduction of a small amount of Ce leads to a noticeable decrease in Er-related energy deposition, indicating that Ce co-doping effectively alleviates the deposited energy away from the vicinity of Er ions. With further increasing Ce concentration, the Er-related energy

deposition begins to increase, indicating the presence of an optimal Ce concentration. Moreover, the optimal Ce concentration shifts toward higher values as the Er concentration increases, indicating a concentration-matching relationship between Er and Ce.

This phenomenon is associated with the generation and transport of secondary particles during irradiation. At low Ce concentrations, Ce co-doping redistributes part of the deposited energy away from the vicinity of Er ions. In contrast, excessive Ce doping enhances the interaction between γ-rays and the fiber material, resulting in the generation of more Compton electrons and other secondary particles. As a result, more secondary particles interact with Er ions, leading to higher local energy deposition around Er ions. Consequently, the optimal Ce concentration varies with the Er concentration. Only by properly matching the Er/Ce concentration ratio can an optimal balance be achieved between reducing local energy deposition around Er ions and suppressing secondary-particle effects, thereby maximizing the radiation resistance of Er/Ce co-doped fibers.

The optimized core composition identified in Group 1 (0.6 wt% Er and 0.3 wt% Ce) was adopted to evaluate the effect of the Ce-doped cladding on energy deposition. The simulation parameters are listed in Group 2 of Table 1, and the corresponding results are presented in Figure 3. A cladding Ce concentration of 0 wt% and a cladding thickness of 0 μm correspond to the reference fiber without Ce-doped cladding. At a cladding thickness of 15 μm and a Ce concentration of 1 wt%, the core energy deposition reaches a minimum of 11.43 MeV, corresponding to a reduction of approximately 9.2% compared with the reference structure. For a given Ce concentration, core energy deposition first decreases and then increases with increasing cladding thickness. An analogous trend is observed when the Ce concentration is varied at a fixed cladding thickness. Therefore, the optimal Ce concentration is not a constant value. For relatively thin cladding layers, a higher Ce concentration is needed to minimize core energy deposition. As the cladding becomes thicker, the optimal Ce concentration shifts toward lower values. These results indicate that both the Ce concentration and the cladding thickness determine the amount of Ce participating in radiation interactions. Consequently, the radiation-shielding performance of the Ce-doped cladding depends on the combined effect of these two parameters, both of which should be considered when designing radiation-resistant optical fibers.

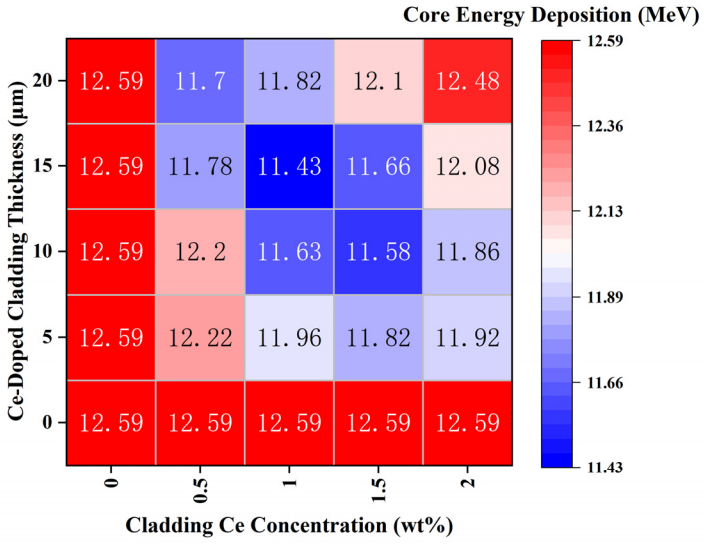


Figure 3. Two-dimensional distribution of core energy deposition as a function of cladding Ce concentration and Ce-doped cladding thickness.

The Er and Ce concentration ranges adopted in the initial GEANT4 simulations are higher than those used in the fabricated fibers. Since the experimentally achievable dopant

concentrations are relatively low, the corresponding variation in radiation energy deposition becomes less pronounced, making the influence of dopant concentration difficult to distinguish. Therefore, broader Er and Ce concentration ranges were initially employed to clearly reveal the relationship between dopant distribution and radiation energy deposition. However, in practical fiber fabrication, the dopant concentrations cannot be arbitrarily increased because excessive rare-earth or co-dopant concentrations may lead to ions clustering, and deterioration of fiber fabrication quality. Therefore, experimentally achievable doping levels need to be considered when designing radiation-resistant fibers.

To verify whether the trends observed in the broad concentration range remain valid under practical fabrication conditions, additional GEANT4 simulations were performed in the low-concentration regime. As shown in Figure 4, both the experimentally adopted core Ce concentration (0.028 wt%) and cladding Ce concentration (0.17 wt%) are located within the effective energy-deposition reduction regions, as highlighted by the red pentagrams. The variation trends are consistent with those observed in the broader concentration range, further supporting the effectiveness of the proposed core–cladding Ce co-doped structure for improving radiation resistance.

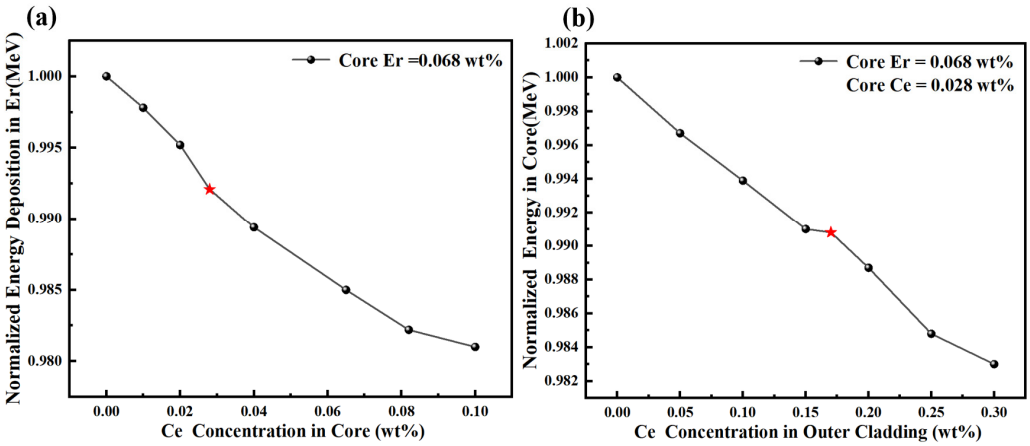


Figure 4. GEANT4 simulation results in the low-concentration range. (**a**) Normalized energy deposited in Er ions versus core Ce concentration. (**b**) Normalized energy deposited in the fiber core versus outer-cladding Ce concentration. The asterisk (★) indicates the experimentally fabricated Ce concentration.

The low-concentration simulations confirm that the experimentally adopted Ce concentrations remain within the effective reduction region identified by the broader parametric study. The present results support the feasibility of the proposed core–cladding Ce co-doping structure under experimentally achievable doping conditions. Future work will focus on optimizing the Ce concentration and distribution within experimentally achievable doping ranges to further improve radiation resistance.

To further clarify the influence of Ce-doped cladding on the radial energy deposition distribution, the energy deposition along the radial direction from the fiber core to the outer cladding was extracted from the GEANT4 simulation. The energy deposition in the core region was normalized to 1, and the relative energy deposition distribution from the core center to the cladding boundary was analyzed.

As shown in Figure 5, the normalized energy deposition at the fiber core is defined as 1 because the core contains the Er-doped region where most radiation interactions occur. The normalized energy deposition at other radial positions therefore represents the relative energy deposition with respect to the fiber core. Compared with the conventional EDF, the fiber with Ce-doped cladding exhibits a noticeably lower normalized energy deposition in the core region. Specifically, the normalized energy deposition at the fiber

center decreases from 1.00 for the conventional EDF to approximately 0.72 after introducing the Ce-doped cladding, corresponding to a reduction of about 28%. This result indicates that less radiation energy is deposited around the Er-doped core, which is beneficial for suppressing radiation-induced defect formation. Outside the core region, both structures exhibit fluctuations in normalized energy deposition due to the transport, scattering, energy loss, and re-deposition of radiation-induced secondary electrons within the silica matrix.

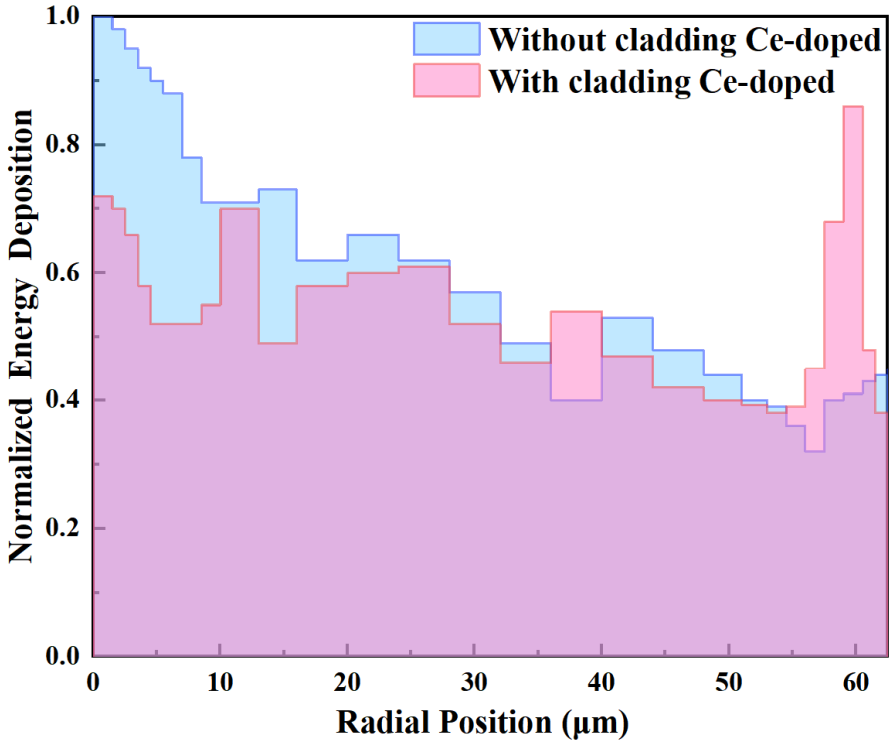


Figure 5. Radial redistribution of radiation-induced energy deposition in Ce-doped core–cladding fiber structure.

A more pronounced difference appears near the outer cladding region. As the radial position approaches the Ce-doped cladding layer (approximately 57.5–62.5 μm), the normalized energy deposition of the Ce-containing structure increases significantly, reaching approximately 0.68–0.86, whereas the conventional EDF remains at approximately 0.32–0.43 over the same radial range. This redistribution demonstrates that part of the radiation energy is transferred from the fiber core toward the Ce-doped cladding instead of remaining concentrated within the Er-doped core.

Considering that the penetration range of keV-level electrons in SiO_2 is typically limited to several micrometers, the effect of cladding Ce should be understood as a localized modulation of electron scattering and energy deposition rather than direct electron shielding. The radial energy deposition results provide direct evidence that Ce-containing cladding can alter the spatial distribution of radiation energy deposition and reduce the energy accumulation in the core region, which contributes to the improved radiation resistance of CEDF structures.

3. Experimental Results and Discussion

3.1. Fiber Fabrication and Irradiation Conditions

Three EDF samples with different Ce-doping configurations were prepared using the modified chemical vapor deposition (MCVD) process combined with solution doping [24,25]. Their elemental compositions and geometric parameters are summarized

in Table 3. The three fibers exhibited comparable dimensions, with core diameters of approximately 8.6 μm, 8.4 μm, and 8.5 μm for EDF, CEDF1, and CEDF2, respectively, while all samples shared a cladding diameter of 125 μm. The Er concentrations were maintained within a comparable range of approximately 0.06–0.07 wt% among all fibers. CEDF1 and CEDF2 contained the same core Ce concentration of 0.028 wt%, whereas CEDF2 further incorporated a Ce-doped cladding layer with a Ce concentration of 0.17 wt%, forming the proposed core–cladding Ce co-doped structure. Besides Er and Ce, Ge, Al, and P were also introduced to tailor the refractive-index profile and spectroscopic properties of the fiber core, and their concentrations are listed in Table 3. The core doping was primarily achieved through MCVD combined with solution doping, while the Ce-doped cladding layer was introduced by incorporating Ce-doped silica sleeves during preform fabrication. The relatively short heat treatment time and controlled fabrication parameters in the MCVD process effectively minimize excessive dopant migration between the core and cladding regions. It should be noted that the fabrication repeatability and compositional uniformity of the prepared fiber samples require further statistical verification.

Table 3. Main parameters of fiber samples.

Fiber Parameters	EDF	CEDF1	CEDF2
Core/cladding diameter (μm)	8.6/125	8.4/125	8.5/125
Core Er (wt%)	0.070	0.068	0.061
Core Ce (wt%)	0	0.028	0.028
Cladding Ce (wt%)	0	0	0.170
Ge (wt%)	4.476	5.206	5.665
Al (wt%)	0.632	0.523	0.541
P (wt%)	1.48	2.240	2.364

Gamma-irradiation experiments were conducted using a ^{60}Co source at the Zhongxin Irradiation Center in Qingdao, China. All irradiations were performed at room temperature with a dose rate of approximately 700–800 Gy/h. The total irradiation doses were set to 300 Gy, 600 Gy, and 1200 Gy, respectively. It should be noted that the radiation environment in practical space missions is highly complex, involving multiple particle species (e.g., trapped protons/electrons, solar particles, and heavy ions [26]), various dose rates, and additional environmental factors such as vacuum and thermal cycling. The ^{60}Co γ-ray irradiation employed in this work does not aim to fully reproduce the orbital radiation environment, but rather serves as a controlled and repeatable method to evaluate the relative radiation tolerance of different fiber structures and investigate the radiation-induced degradation mechanisms.

3.2. Gain Spectra

The amplification performance of EDF, CEDF1, and CEDF2 was characterized using a forward-pumping configuration. A 980 nm laser was used as the pump source with a pump power of 800 mW, while the input signal power was fixed at −20 dBm. The corresponding C-band gain spectra are presented in Figure 6. All three fibers exhibited stable amplification across the C-band. At 1550 nm, the maximum gains of EDF, CEDF1, and CEDF2 reached 24.14 dB, 27.27 dB, and 24.71 dB, respectively. These results indicate that the introduction of Ce does not adversely affect the amplification performance of erbium-doped fibers. Among the three samples, CEDF1 achieved the highest gain, whereas CEDF2 retained a comparable amplification level despite the introduction of the Ce-doped cladding. The slightly lower gain of CEDF2 is likely caused by additional pump or signal attenuation introduced by the

Ce-doped cladding layer. The measurement uncertainty of the gain mainly originates from pump power fluctuation, optical coupling variation, and spectral acquisition noise.

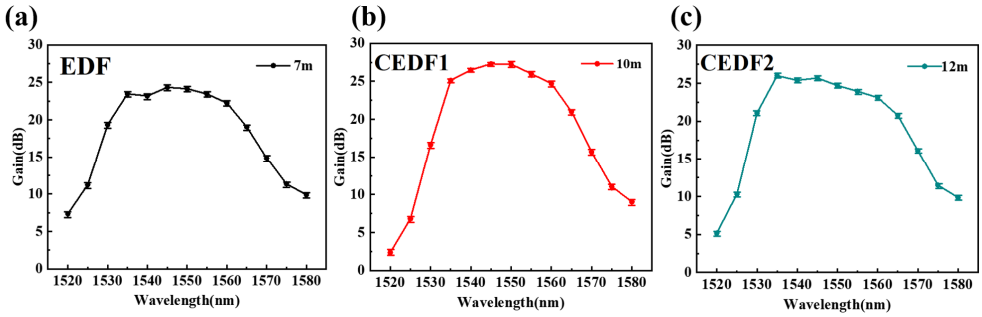


Figure 6. Gain spectra of EDF, CEDF1, and CEDF2 before irradiation under 980 nm pumping conditions. (**a**) EDF. (**b**) CEDF1. (**c**) CEDF2.

3.3. Radiation-Induced Absorption

Figure 7 compares the absorption spectra before and after γ-ray irradiation together with the corresponding RIA spectra. Figure 7a–c show the absorption spectra, whereas Figure 7d–f present the corresponding RIA spectra obtained by subtracting the pre-irradiation spectra from the post-irradiation spectra. The RIA decreases with increasing wavelength, with substantially higher absorption observed in the short-wavelength region than in the long-wavelength region. This behavior is attributed to Al-related radiation-induced defect centers in the silica matrix [27]. For all three fibers, the RIA increases with irradiation dose, reflecting the progressive accumulation of radiation-induced defects. Both CEDF1 and CEDF2 exhibit lower RIA than conventional EDF at all irradiation doses, confirming the effectiveness of Ce co-doping in suppressing radiation-induced defect formation. After irradiation to 1200 Gy, the RIA at 1200 nm is 6.91 dB/m for EDF, 4.98 dB/m for CEDF1, and 4.11 dB/m for CEDF2. Relative to EDF, the RIA decreases by approximately 27.9% and 40.5% for CEDF1 and CEDF2, respectively. The observed trend agrees well with the energy-deposition characteristics predicted by the GEANT4 simulations. This result confirms the effectiveness of the proposed core–cladding Ce co-doped design in improving the radiation resistance of erbium-doped fibers.

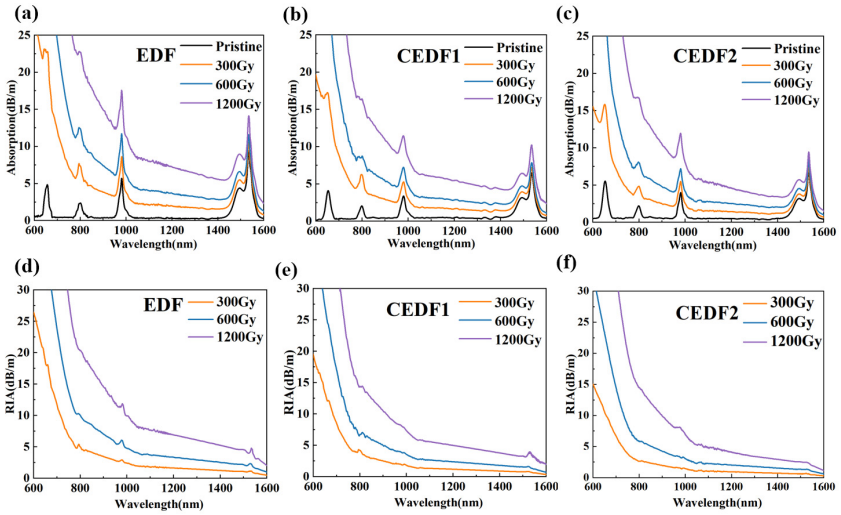


Figure 7. Absorption spectra and corresponding radiation-induced absorption (RIA) spectra of EDF, CEDF1, and CEDF2 under different γ-ray irradiation doses: (**a**,**d**) EDF; (**b**,**e**) CEDF1; and (**c**,**f**) CEDF2.

3.4. Radiation-Induced Gain Variation

The radiation-induced gain variation (RIGV) was calculated according to Equation (3):

$$\mathrm{RIGV} = G_{\mathrm{before}} - G_{\mathrm{after}} \tag{3}$$

where G_{before} and G_{after} represent the fiber gain before and after irradiation, respectively. The uncertainty of RIGV mainly results from the accumulated errors of the gain measurements before and after irradiation, including pump fluctuation and measurement noise. The optimal fiber length of each sample was first determined based on its amplification performance. The radiation-induced degradation was then evaluated using the same fiber length before and after irradiation for each sample. Therefore, the calculated gain variation reflects the relative radiation-induced degradation of each fiber structure, which provides a more direct evaluation of the radiation resistance rather than the absolute gain difference caused by slight variations in Er concentration.

Figure 8 presents the RIGV at 1550 nm as a function of pump power for EDF, CEDF1, and CEDF2 under different irradiation doses. At a given pump power, the RIGV of all three fibers increases with irradiation dose, reflecting the progressive degradation of radiation tolerance, consistent with previous reports. RIGV decreases with pump power and approaches a plateau above approximately 300 mW. Under the 1200 Gy irradiation condition, increasing the pump power from 50 mW to 500 mW reduces the RIGV from 10.3 dB to 5.2 dB for EDF, from 6.2 dB to 3.75 dB for CEDF1, and from 3.5 dB to 2.18 dB for CEDF2. At higher pump powers, enhanced photobleaching and thermal bleaching help mitigate radiation-induced gain degradation [28,29]. However, the reduction in RIGV becomes progressively smaller as the pump power continues to increase, suggesting that the photobleaching effect gradually reaches saturation. Across the investigated dose range, both CEDF1 and CEDF2 exhibit lower RIGV than conventional EDF, with CEDF2 consistently showing the smallest gain variation. At an irradiation dose of 1200 Gy and a pump power of 50 mW, the RIGV of CEDF2 is 58.1% lower than that of EDF. This trend is consistent with the RIA results, confirming that Ce co-doping effectively mitigates RIGV. The additional introduction of Ce into the cladding further enhances this effect, leading to the highest radiation tolerance among the three fibers.

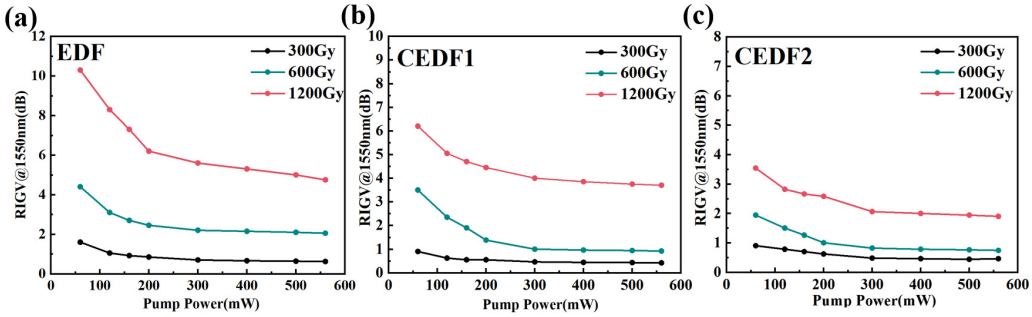


Figure 8. Radiatio Radiation-induced gain variation (RIGV) characteristics under different irradiation doses. (**a**) EDF. (**b**) CEDF1. (**c**) CEDF2.

In this work, RIA and RIGV at 1550 nm were selected as the main evaluation parameters because 1550 nm is a representative wavelength in the C-band and enables direct comparison of radiation-induced degradation among different fiber structures. Nevertheless, practical EDFA applications require further evaluation of system-level parameters, including noise figure, C-band gain flatness, pump efficiency, output power stability, and post-irradiation recovery behavior. These parameters were beyond the scope of the present

study and will be investigated in future work to further evaluate the practical applicability of the proposed radiation-resistant fibers.

4. Discussion

The significant reductions in RIA and RIGV achieved by the proposed core–cladding Ce co-doping structure are expected to improve the long-term gain stability and operational reliability of erbium-doped fiber amplifiers operating in radiation environments, demonstrating its potential for radiation-hardened space optical communication systems.

Future work will focus on further optimizing the Ce concentration and distribution to achieve improved radiation resistance within experimentally achievable doping ranges. It should also be noted that, besides Ce, slight variations in Ge, Al, P, and Er concentrations among different fiber samples may influence defect formation and radiation-induced degradation behavior. Therefore, their contributions cannot be completely excluded. However, the consistent improvement observed after introducing core–cladding Ce co-doping indicates that Ce incorporation and distribution are considered to be the primary contributors to the enhanced radiation resistance. A more comprehensive evaluation of the engineering applicability of the proposed fibers will require further investigation of intrinsic optical properties, including background loss, fluorescence lifetime, and quantum efficiency. Furthermore, validation under low-dose-rate and mixed-particle irradiation conditions representative of practical space environments will be carried out in future studies.

5. Conclusions

In this work, GEANT4 Monte Carlo γ-ray irradiation models were constructed to systematically investigate Er/Ce concentration ratio in fiber cores, as well as the synergistic influence of Ce-doped cladding concentration and thickness on core-localized energy deposition. The simulation results indicate that Ce co-doping can effectively reduce the local energy deposition around Er ions. However, the optimal Ce concentration is not a fixed value and varies with the Er concentration. Furthermore, the introduction of a Ce-doped cladding provides additional suppression of energy deposition in the fiber core and exhibits a distinct concentration–thickness synergistic optimization effect. The results demonstrate that the energy-deposition distribution within the fiber is jointly determined by the Ce concentration and thickness of the cladding, with the minimum energy deposition occurring within an optimized parameter region formed by their combined influence.

Based on the simulation results, EDF, CEDF1, and CEDF2 were fabricated using MCVD process combined with solution doping. The compositional designs of CEDF1 and CEDF2 were selected according to the low-energy-deposition regions identified by the simulations. Gamma irradiation experiments were subsequently carried out at total doses of 300 Gy, 600 Gy, and 1200 Gy. At 1200 Gy, the RIA of CEDF1 and CEDF2 were reduced by approximately 27.9% and 40.5%, respectively, compared with that of conventional EDF. After irradiation, all fiber samples exhibited varying degrees of gain degradation, while CEDF2 showed the best gain stability. Under a total dose of 1200 Gy, the RIGV of CEDF2 decreased to 2.18 dB, corresponding to a reduction of approximately 58.1% relative to EDF.

The experimental results are consistent with the energy-deposition behavior predicted by the GEANT4 simulations and with the observed RIA characteristics, demonstrating that the proposed core–cladding Ce co-doped structure can effectively reduce radiation energy deposition in the fiber core and suppress the degradation induced by radiation-generated defects. These findings suggest that optimizing the spatial distribution of Ce ions in both the core and cladding regions is an effective strategy for further improving the radiation resistance of erbium-doped fibers, providing valuable guidance for the development of radiation-hardened erbium-doped fibers and related fiber amplifiers.

https://doi.org/10.3390/photonics13080727

Author Contributions: Conceptualization, W.C.; methodology, Y.X. and W.F.; software, Y.X.; validation, Y.X. and W.F.; formal analysis, Y.X.; investigation, Y.X.; resources, W.C.; data curation, Y.X.; writing—original draft preparation, Y.X.; writing—review and editing, Z.X., R.F., T.Y., W.F. and W.C.; visualization, Y.X.; supervision, W.C.; project administration, W.C.; funding acquisition, W.C. All authors have read and agreed to the published version of the manuscript.

Funding: This work was supported by the National Natural Science Foundation of China (Grant No. 62275148), the Science and Technology Project of State Grid Corporation of China (Grant No. 52180026001A-206-ZN), the Shandong Province Technology Innovation Guidance Plan (Grant No. YDZX2025010), the Shanghai Qiyuan State-owned Assets Pioneer Project (Grant No. QY2025-GZ-004), and the National Key R&D Projects (Grant No. 2023YFB3610703).

Institutional Review Board Statement: Not applicable.

Informed Consent Statement: Not applicable.

Data Availability Statement: The data presented in this study are available from the corresponding author upon reasonable request.

Acknowledgments: The authors would like to thank Wei Chen for his valuable guidance and support throughout this work.

Conflicts of Interest: Author Yangjian Xu, Ziyang Xiao, Wenju Feng, Ruixiang Fan, Tao Yang, and Wei Chen are employed by the company State Grid Jiangxi Electric Power Co., Ltd., Nanchang 330077, China. All authors declare that the research was conducted in the absence of any commercial or financial relationships that could be construed as a potential conflict of interest.

Abbreviations

The following abbreviations are used in this manuscript:

EDF	Erbium-Doped Fiber
EDFA	Erbium-Doped Fiber Amplifier
CEDF1	core Ce co-doped EDF
CEDF2	Core–Cladding Ce co-doped EDF
RIA	Radiation-Induced Absorption
RIGV	Radiation-Induced Gain Variation
MCVD	Modified Chemical Vapor Deposition
CERN	European Organization for Nuclear Research

References

1. Zyskind, J. Erbium-Doped Fiber Amplifiers: What Everyone Needs to Know. In Proceedings of the Optical Fiber Communication Conference and Exhibition (OFC), Anaheim, CA, USA, 20–24 March 2016; pp. 1–135.
2. Logan, R.; Basuita, D. Photonic Components for Spacecraft Fiber Optic Datalinks and Free-Space Optical Communications Terminals. In Proceedings of the International Conference on Space Optics (ICSO), Online, 30 March–2 April 2021; Paper 1185244.
3. Girard, S.; Morana, A.; Ladaci, A.; Robin, T.; Mescia, L.; Bonnefois, J.-J.; Boutillier, M.; Mekki, J.; Paveau, A.; Cadier, B.; et al. Recent Advances in Radiation-Hardened Fiber-Based Technologies for Space Applications. *J. Opt.* **2018**, *20*, 093001. [CrossRef]
4. Deng, Y.; Jiang, J. Optical Fiber Sensors in Extreme Temperature and Radiation Environments: A Review. *IEEE Sens. J.* **2022**, *22*, 13811–13834. [CrossRef]
5. Ma, J.; Li, M.; Tan, L.-Y.; Zhou, Y.-P.; Yu, S.-Y.; Che, C. Space Radiation Effect on EDFA for Inter-Satellite Optical Communication. *Optik* **2010**, *121*, 535–538. [CrossRef]
6. Benton, E.R.; Benton, E.V. Space Radiation Dosimetry in Low-Earth Orbit and Beyond. *Nucl. Instrum. Methods Phys. Res. B* **2001**, *184*, 255–294. [CrossRef] [PubMed]
7. Girard, S.; Kuhnhenn, J.; Gusarov, A.; Morana, A.; Paillet, P.; Robin, T.; Weninger, L.; Fricano, F.; Roche, M.; Campanella, C.; et al. Overview of Radiation Effects on Silica-Based Optical Fibers and Fiber Sensors. *IEEE Trans. Nucl. Sci.* **2025**, *72*, 982–1020. [CrossRef]
8. Brichard, B.; Fernandez, A. Radiation Effects in Silica Glass Optical Fibers. In Proceedings of the RADECS Conference, Cap d'Agde, France, 19–23 September 2005; pp. 95–138.

9. Li, J.; Chen, Q.; Zhou, J.; Cao, Z.; Li, T.; Liu, F.; Yang, Z.; Chang, S.; Zhou, K.; Ming, Y.; et al. Radiation Damage Mechanisms and Research Status of Radiation-Resistant Optical Fibers: A Review. *Sensors* **2024**, *24*, 3235. [CrossRef] [PubMed]
10. Dardaillon, R.; Lancry, M.; Myara, M.; Palermo, C.; Signoret, P. Radiation-Induced Absorption and Photobleaching in Erbium Al-Ge Codoped Optical Fiber. *J. Mater. Sci.* **2020**, *55*, 14326–14335. [CrossRef]
11. Ding, M.J.; Wei, S.E.; Luo, Y.H.; Peng, G.-D. Reversible Photo-bleaching Effect in a Bismuth/Erbium Co-Doped Optical Fiber under 830 nm Irradiation. *Opt. Lett.* **2016**, *41*, 4688–4691. [CrossRef] [PubMed]
12. Wu, X.; Liu, C.-X.; Wu, D.; Li, M.; Ruan, S.-C. Radiation Resistance of an Er/Ce Codoped Superfluorescent Source of Conventional Fiber and Photonic Crystal Fiber. *Opt. Eng.* **2017**, *56*, 126109. [CrossRef]
13. Friebele, E.J. Radiation Protection of Fiber Optic Materials: Effect of Cerium Doping on Radiation-Induced Absorption. *Appl. Phys. Lett.* **1975**, *27*, 210–212. [CrossRef]
14. Sheng, Y.B.; Yang, L.; Luan, H.; Liu, Z.; Yu, Y.; Li, J.; Dai, N. Improvement of Radiation Resistance by Introducing CeO_2 in Yb-Doped Silicate Glasses. *J. Nucl. Mater.* **2012**, *427*, 58–61. [CrossRef]
15. Jiao, Y.; Shao, C.; Guo, M.; Guzik, M.; Zhang, Y.; Yu, C.; Boulon, G.; Hu, L. Influence of Ce^{3+} Ion on Optical Properties and Radiation Resistance in Ce^{3+}/Tm^{3+} Co-Doped Aluminosilicate Glasses. *Opt. Mater. X* **2022**, *13*, 100113. [CrossRef]
16. Girard, S.; Laurent, A.; Pinsard, E.; Robin, T.; Cadier, B.; Boutillier, M.; Marcandella, C.; Boukenter, A.; Ouerdane, Y. Radiation-Hard Erbium Optical Fiber and Fiber Amplifier for Both Low- and High-Dose Space Missions. *Opt. Lett.* **2014**, *39*, 2541–2544. [CrossRef] [PubMed]
17. Girard, S.; Vivona, M.; Laurent, A.; Cadier, B.; Marcandella, C.; Robin, T.; Pinsard, E.; Boukenter, A.; Ouerdane, Y. Radiation Hardening Techniques for Er/Yb-Doped Optical Fibers and Amplifiers for Space Application. *Opt. Express* **2012**, *20*, 8457–8465. [CrossRef] [PubMed]
18. Cao, C.; Gu, Z.; Qiu, Q.; He, L.; Chu, Y.; Xing, Y.; Dai, N.; Li, J. Radiation-Resistant Er-Doped Fiber Based on Ge-Ce Co-Doping. *IEEE Photonics J.* **2022**, *14*, 7146605. [CrossRef]
19. Yaghi, M.A.; Sayyed, M.I.; Mhareb, M.H.; Bennal, A.S.; Hamad, M.K. Radiation Shielding and Mechanical Performance of Lead-Free Novel Glasses: Insights from Geant4 Monte Carlo Simulations. *Radiat. Phys. Chem.* **2025**, *239*, 113335. [CrossRef]
20. Facchini, A.; Morana, A.; Mescia, L.; Campanella, C.; Shuvo, M.M.; Robin, T.; Marin, E.; Ouerdane, Y.; Boukenter, A.; Girard, S. Experimental–Simulation Analysis of a Radiation Tolerant Erbium-Doped Fiber Amplifier for Space Applications. *Appl. Sci.* **2023**, *13*, 11589. [CrossRef]
21. Griscom, D.L. Optical Properties and Structure of Defects in Silica Glass. *J. Ceram. Soc. Jpn.* **1991**, *99*, 923–942. [CrossRef]
22. Devine, R.A.B.; Francou, J.M. Extrinsic- and Intrinsic-Defect Creation in Amorphous SiO_2. *Phys. Rev. B* **1990**, *41*, 12882–12887. [CrossRef] [PubMed]
23. Skuja, L. Defect Studies in Vitreous Silica and Related Materials: Optically Active Oxygen-Deficiency-Related Centers in Amorphous Silicon Dioxide. *J. Non-Cryst. Solids* **1998**, *239*, 16–48.
24. Poole, S.B.; Payne, D.N.; Mears, R.J.; Fermann, M.; Laming, R. Fabrication and Characterization of Low-Loss Optical Fibers Containing Rare-Earth Ions. *J. Light. Technol.* **1986**, *4*, 870–876. [CrossRef]
25. Dhar, A.; Choudhury, N.; Sen, R. Advancements in Fabrication Technology for Rare-Earth Doped Optical Fibers: A Retrospective Analysis. *Opt. Commun.* **2025**, *577*, 131463. [CrossRef]
26. Brunetti, G.; Campiti, G.; Tagliente, M.; Ciminelli, C. COTS Devices for Space Missions in LEO. *IEEE Access* **2024**, *12*, 76478–76514. [CrossRef]
27. Deschamps, T.; Vezin, H.; Gonnet, C.; Ollier, N. Evidence of AlOHC Responsible for the Radiation-Induced Darkening in Yb-Doped Fiber. *Opt. Express* **2013**, *21*, 8382–8392. [CrossRef] [PubMed]
28. Ladaci, A.; Girard, S.; Mescia, L.; Laurent, A.; Ranger, C.; Kermen, D.; Robin, T.; Cadier, B.; Boutillier, M.; Sane, B.; et al. Radiation-Hardened High-Power Er^{3+}/Yb^{3+} Co-Doped Fiber Amplifiers for Free-Space Optical Communications. *Opt. Lett.* **2018**, *43*, 3049–3052. [PubMed]
29. Schuyt, J.J.; Duke, O.; Moseley, D.A.; Ludbrook, B.M.; Salazar, E.E.; Badcock, R.A. Gamma Irradiation of Ge-Doped and Radiation-Hard Silica Fibers at Cryogenic Temperatures: Mitigating Radiation-Induced Attenuation with 1550 and 970 nm Photobleaching. *J. Appl. Phys.* **2023**, *134*, 043103. [CrossRef]

Disclaimer/Publisher's Note: The statements, opinions and data contained in all publications are solely those of the individual author(s) and contributor(s) and not of MDPI and/or the editor(s). MDPI and/or the editor(s) disclaim responsibility for any injury to people or property resulting from any ideas, methods, instructions or products referred to in the content.